Received 18 May 2022; revised 13 June 2022; accepted 7 July 2022. Date of publication 8 August 2022; date of current version 12 August 2022.

Digital Object Identifier 10.1109/OJAP.2022.3191019

A Compact Wideband Antenna With an Orthogonal Radiating Choke for Broadside Gain Enhancement

LIDONG CHI [1] (Graduate Student Member, IEEE), YIHONG QI [1,2] (Senior Member, IEEE), FRANCESCO DE PAULIS [3] (Senior Member, IEEE), AND YUEPING ZHANG [4] (Fellow, IEEE)

[1]School of Electrical and Information Engineering, Hunan University, Changsha 410000, China

[2]LinkE Technologies (Hengqin) Company Ltd., Hengqin 519031, China

[3]UAq EMC Laboratory, Department of Industrial and Information Engineering and Economics, University of L'Aquila, 67100 L'Aquila, Italy

[4]Department of Electrical and Electronic Engineering, Nanyang Technological University, Singapore 639798

CORRESPONDING AUTHOR: Y. QI (e-mail: yihongqi@gmail.com)

This work was supported in part by the Chinese Ministry of Education–China Mobile Research Foundation under Grant MCM20150101, and in part by the National Natural Science Foundation of China under Grant 61671203.

ABSTRACT A broadband compact antenna is proposed in this paper with an enhanced broadside gain performances in the +/− z directions. A design method of complementary gains is presented to overcome the gain reduction caused by the cancellation of reverse currents in the middle of the band of interest, where a design equation of the excited element of the antenna is given. This objective is achieved by accurately analyzing the resonant modes of the two parallel connected antennas of the excited element in order to achieve an overall wideband radiator. An orthogonal radiating choke (ORC) is proposed to remove the gain depression due to the leakage of electromagnetic waves toward the upper portion of the band of interest through simultaneously enhancing the broadside gain and choking the end-fire travelling wave. Each one patch of the ORC acting as both a TM_{10} mode microstrip antenna and a choke of end-fire travelling wave. With the help of the ORC, the gain in +/− z directions is enhanced by 13.1 dB at 6 GHz compared to that without the ORC. The proposed antenna presents a realized broadside gain of 2.1-7.8 dBi in the +/− z directions within a bandwidth of 158% (700 MHz – 6 GHz). Both the simulated and measured results demonstrate that the proposed antenna exhibits desirable bandwidth and gain characteristics and is a promising candidate for broadband integrated wireless systems.

INDEX TERMS Broadband, broadside, gain, bandwidth, leakage.

I. INTRODUCTION

BROADSIDE antennas are popular with various applications for wireless communications due to its low profile and easy integration [1]–[3]. The current 5G NR (New Radio) requires a band covering 700 MHz - 5 GHz (more than 150% relative bandwidth), which imposes a new ultra-wide bandwidth requirement for broadside antennas [4]–[6]. Since the antenna size varies significantly with frequency, it is difficult to achieve stable broadside radiation in the wide band of interest [7].

Two main factors affect the bandwidth of the broadside radiation, the first one is due to the driven element, whereas the second is a consequence of the reflector [8]. By considering impedance matching and gain enhancement, the maximum fractional bandwidth of a planar reflector is generally 90%, where the distance of the reflector from the radiating element goes from 1/8λ to 1/3λ. With the objective of excluding the influence of the reflector, this paper focuses on the bandwidth of the excited element, such as an omni-directional and bilateral broadside antenna. The broadside gain decrease generally comes from the cancellation of reversed currents (CRC) (mainly at low frequencies) and the leakage of electromagnetic waves (LEW) (mainly in the high frequency band). The LEW is the presence of a travelling wave, specifically a surface wave, that is degrading the radiating performance. By relying on only one single type of traditional classic antennas it is hard to achieve an effective gain characteristic in a broad band [9]–[11]. In order to

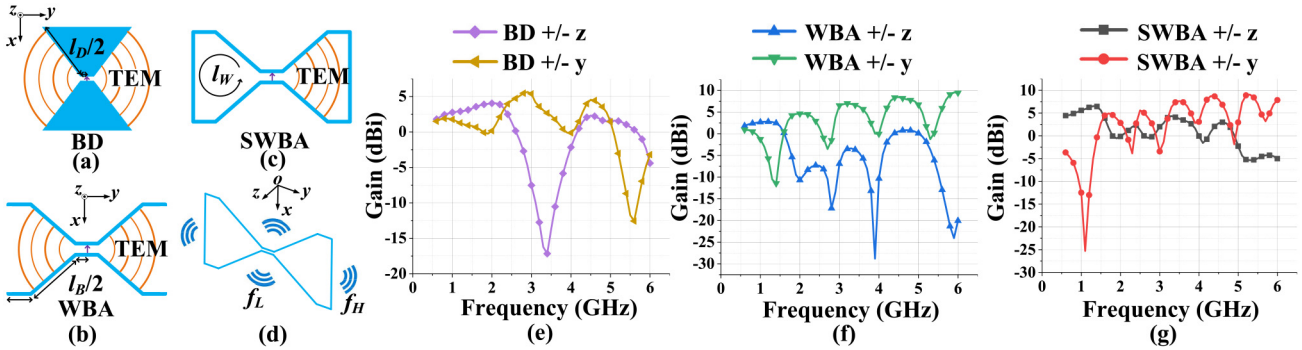

FIGURE 1. (a) Front view of the BD. (b) Front view of the WBA. (c) Front view of the SWBA. (d) Oblique view of the SWBA. Simulated gains of (e) the BD, (f) the WBA, and (g) the SWBA in the broadside (+/−z) and the end-fire (+/−y) directions.

limit the gain degradation due to the CRC, antennas with hybrid modes have been developed [9]–[14]. The work in [9] proposed a monopole-fed slot-loop hybrid antenna obtaining a 4.0-5.3 dBi broadside gain within a 102.9% bandwidth, where a loop mode, a slot mode, and a monopole mode work in the lower band, in the middle band, and in the higher band, respectively. An antenna consisting of a symmetrical dipole and an antipodal loop was proposed in [14], which achieves a −2-6 dBi peak gain in a 129% bandwidth. On the other side of the band of interest, instead, to compensate for the gain depression led by the LEW, a dipole with metasurface containing index-gradient patches was proposed reaching a 2.1-7.3 dBi broadside gain within a 131% bandwidth [15]. The metasurface effectively suppresses the travelling wave. However, the bandwidth is limited by the CRC, since the length of the dipole at highest frequency is 3/2λ, where the gain decreases to 0 dBi.

Compared with dipole antennas, a shorted wire biconical antenna (SWBA), also denoted as a wideband high efficiency electromagnetic structure (WHEMS), is able to achieve a higher broadside gain of 6 dBi at the 3/2λ resonant mode due to the bending and the short circuit processes [16]. However, in the lower side of the band, the antenna works at the λ resonant mode, where the dimension is large. Moreover, the SWBA still has gain depression due to the CRC and the LEW.

An antenna, which is based on the combination of the SWBA, the X-shape bowtie dipole (BD), and the patches, with wideband broadside gain characteristics is proposed in this paper to solve the problems led by the CRC and the LEW. A design method of complementary gains will be presented to enhance the gain degradation caused by the CRC, where a design equation of the excited element is given. An orthogonal radiating choke (ORC) is to be proposed to fix the gain depression due to the LEW through simultaneously enhancing the broadside gain and choking the end-fire travelling wave.

II. MODE ANALYSIS AND DESIGN OF THE EXCITED ELEMENT

In this section, a design method of complementary gains is applied for devising the excited element based on an accurate mode analysis of three elementary radiators. Furthermore, a design equation of the excited element is provided for lowest working frequency calculation and outline determination.

A. BASIC WORKING PRINCIPLES OF THE ELEMENTARY RADIATORS

The proposed wideband antenna is achieved by combining appropriately more radiating elements such that a wider band and high gain is obtained. The electromagnetic radiating principles of three types of elementary antennas are studied in this subsection to clearly explain how their combination can effectively led to the target antenna performances. Fig. 1(a)–(d) show the BD, the wire biconical antenna (WBA), and the SWBA since their working principles are relevant for achieving the final design. The three antennas have a common taper slot that is guiding the TEM principal mode of operation [17]. However, differences occur among them; the boundary conditions of the BD and the WBA are both open circuited thus they resemble more those of a dipole type of antenna, whereas the boundary conditions of the SWBA is of short-circuit type. The short-circuiting of the wire ends leads to two obvious benefits:

1) The shorting arms increase the gain in the +/− z directions at low frequency, where the currents on the arms are in phase with those on the central part of the antenna.

2) The symmetrical short-circuit structure of the antenna forms a voltage balun, which can reduce the common mode currents caused by unbalanced feeding arrangements [18].

Fig. 1(e)–(g) show the gain performance of the three antennas in the broadside (+/− z) and the end-fire (+/− y) directions from 0.6 to 6 GHz, where l_D (λ/2 at 0.70 GHz), l_B (λ/2 at 0.78 GHz), and l_W (λ at 0.95 GHz) are the length of the BD, the length of the WBA, and the perimeter of half of the SWBA slot, respectively. Below 1 GHz, the BD achieves an omni-directional radiation, as demonstrated by the similar values of the gain in the +/− y and +/− z directions. Beyond 1 GHz, the broadside gain and the end-fire gain of the BD can be considered complementary within the band of interest, with a +/− z gain depression at 3.4 GHz caused by the CRC, since the BD is characterized by a 2λ type of resonant mode. A similar result is achieved by the WBA being characterized by an omnidirectional radiation

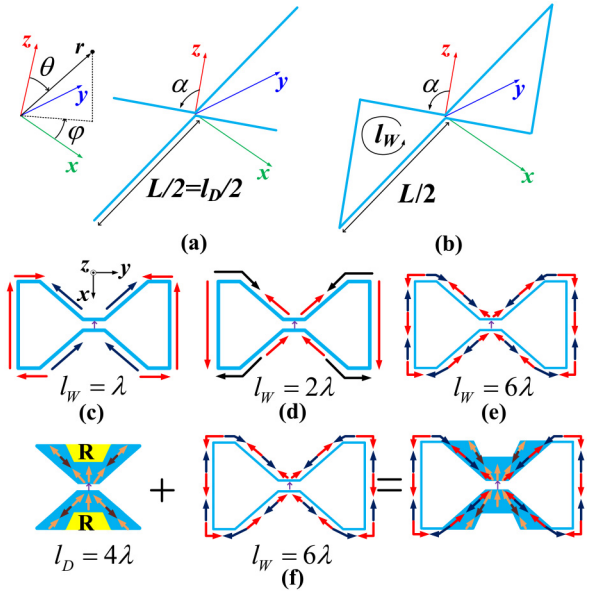

FIGURE 2. Ideal theoretical model of (a) WBA, and (b) SWBA. Current distributions on the SWBA in modes of l_W of (c) λ, (b) 2λ, and (d) 6λ. (e) Current distributions on the BD, the SWBA, and the excited element when l_D and l_W are 4λ and 6λ, respectively.

at 0.6 GHz; a larger gain is obtained at around 1 GHz in the +/− z direction, whereas the radiation in the +/− y direction is predominant beyond 1.6 GHz. The SWBA radiation goes mainly toward the +/−z direction within low frequency bands at frequencies lower than 1.5 GHz, whereas a stronger radiation in the +/− y direction is obtained at frequencies larger than 3.2 GHz. From the results, it appears very challenging to achieve a stable and effective gain in the broadside directions (+/− z) over a bandwidth larger than 150%. Moreover, the SWBA is the most effective radiator in the broadside direction below 5 GHz, compared to the BD and the WBA. Therefore, the SWBA can be combined with other antennas to achieve a broadband broadside antenna.

B. DESIGN OF EXCITED ELEMENT

1) MODE ANALYSIS OF EXCITED ELEMENT

In order to design a broadband active radiating element, the mode analysis of the SWBA is performed herein, and it is combined with the analysis of the radiating features summarized in Section II-A. Fig. 2(a)-(b) show ideal theoretical models of the WBA and the SWBA. The current distributions of the WBA are given in (1),

$$\overrightarrow{I_{WBA}} = \begin{cases} I_0 \sin\left(\frac{\beta L}{2} + \beta l\right) e^{j\beta l(\sin\alpha \sin\theta \sin\varphi + \cos\alpha \cos\theta)} \\ , -\frac{L}{2} \le l \le 0 \\ I_0 \sin\left(\frac{\beta L}{2} - \beta l\right) e^{j\beta l(\sin\alpha \sin\theta \sin\varphi + \cos\alpha \cos\theta)} \\ , 0 \le l \le \frac{L}{2} \\ I_0 \sin\left(\frac{\beta L}{2} + \beta l\right) e^{j\beta l(-\sin\alpha \sin\theta \sin\varphi + \cos\alpha \cos\theta)} \\ , -\frac{L}{2} \le l \le 0 \\ I_0 \sin\left(\frac{\beta L}{2} - \beta l\right) e^{j\beta l(-\sin\alpha \sin\theta \sin\varphi + \cos\alpha \cos\theta)} \\ , 0 \le l \le \frac{L}{2} \end{cases} \quad (1)$$

and the current distributions of the SWBA are presented as (2),

$$\overrightarrow{I_{SWBA}} \begin{cases} I_0 \cos\left(\frac{\beta L(1+\cos\alpha)}{2} + \beta l\right) \\ e^{j\beta l(\sin\alpha \sin\theta \sin\varphi + \cos\alpha \cos\theta)}, -\frac{L}{2} \le l \le 0 \\ I_0 \cos\left(\frac{\beta L(1+\cos\alpha)}{2} - \beta l\right) \\ e^{j\beta l(\sin\alpha \sin\theta \sin\varphi + \cos\alpha \cos\theta)}, 0 \le l \le \frac{L}{2} \\ I_0 \cos\left(\frac{\beta L(1+\cos\alpha)}{2} + \beta l\right) \\ e^{j\beta l(-\sin\alpha \sin\theta \sin\varphi + \cos\alpha \cos\theta)}, -\frac{L}{2} \le l \le 0 \\ I_0 \cos\left(\frac{\beta L(1+\cos\alpha)}{2} - \beta l\right) \\ e^{j\beta l(-\sin\alpha \sin\theta \sin\varphi + \cos\alpha \cos\theta)}, 0 \le l \le \frac{L}{2} \\ I_0 \cos(\beta l) e^{j\beta\left(\frac{L \sin\theta \sin\alpha \sin\phi}{2} + l\cos\theta\right)} \\ , -\frac{L\cos\theta}{2} \le l \le \frac{L\cos\theta}{2} \\ I_0 \cos(\beta l) e^{j\beta\left(-\frac{L \sin\theta \sin\alpha \sin\phi}{2} + l\cos\theta\right)} \\ , -\frac{L\cos\theta}{2} \le l \le \frac{L\cos\theta}{2} \end{cases} . \quad (2)$$

Based on (1) and (2), Fig. 2(c)–(e) show the current distributions of the SWBA corresponding to different resonating modes. When $l_W = 1\lambda$, the currents on the shorting edges are in-phase with that of the taper slot edges thus providing an effective +/− z radiation. Along this broadside direction the gain will be about 3 dB higher than that of the BD and the WBA counterparts. When $l_W = 2\lambda$, the CRC impacts the broadside gain, leading to its reduction as demonstrated by the results in Fig. 1(g) when the frequency is larger than 1.5 GHz. When $l_W = 6\lambda$, the antenna is essentially a travelling wave type of structure that radiates more effectively toward the +/− y directions, thus, the broadside gain is largely degraded by the LEW. From the analysis above some conclusions can be drawn in order to appropriately design the SWBA.

1) The broadside gain of the SWBA is about 3 dB higher than that of the common omni-directional antenna at low frequencies (less than 1.3 GHz); such advantageous behavior should be maintained in the final antenna design.
2) In the intermediate frequency band (1.3 - 5 GHz), the gain decreases at specific bands due to the CRC.
3) At high frequencies (larger than 5 GHz), the SWBA is a travelling wave structure with the travelling TEM wave within the taper slot propagating and radiating to the end-fire directions. The LEW leads to the gain decrease in the +/− z direction.

2) COMPLEMENTARY GAINS DESIGN

The design process of the complementary gains of the excited element is given as follows.

1) Determine the lowest frequency of the band of interest f_L.
2) Let the lowest working frequency of BD cover f_L. l_D is determined.
3) Obtain the lowest frequency $f_{BD\_\min\_L}$ of the minimal gain of the BD.

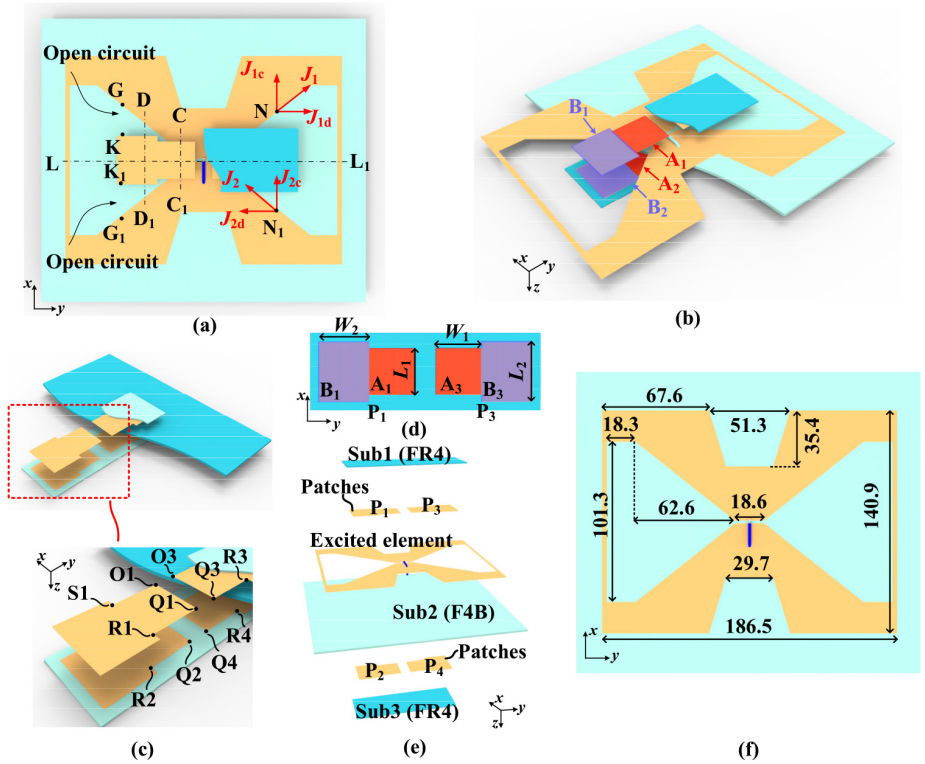

FIGURE 3. Configuration of the proposed antenna. (a) Font view. (b) Global perspective view. (c) Partial perspective view. (d) Radiating patches of P1 and P3. (e) Explosion view. (f) Excited element.

4) Make one of th maximum gain points of the SWBA working at $f_{BD\_\min\_L}$. The selection of the maximum gain point should take into account the gain and impedance characteristics in the broadband. l_W is determined.
5) Parallel connect the BD and the SWBA.

From Fig. 1(e)–(g), the broadside gains of the BD and the SWBA are complementary in the wide band of interest. Thus, the problem of the gain reduction caused by the CRC within the intermediate band can be solved by connecting in parallel the BD and the SWBA. To determine the length of the two radiators, l_D and l_W, respectively, the results in Fig. 1(e)–(g) are considered, and the value of 3.4 GHz is identified where the BD obtains a gain minimum whereas the SWBD achieves a gain maximum. l_D is $\lambda/2$ at 0.70 GHz, and l_W is λ at 0.95 GHz. Thus, based on the geometry of the preliminary designs in Section II-A, a general design guideline can be derived according to (3):

$$l_W / l_D = 1.47. \tag{3}$$

When (3) is satisfied, the BD and the SWBA have a complementary gain below 5 GHz. In addition, by introducing the BD, the excited element can operate at lower frequencies compared to the SWBA, thus leading to a bandwidth expansion to the low frequency range of the band of interest. Let λ_L and λ_H be the wavelength of the lowest and highest frequency of the expanded bandwidth, respectively. When the SWBA is in the lowest resonant mode, l_W is λ, while l_D is calculated 0.68λ using (3). Thus, λ_H is $1.47 l_D$. When the BD is working in the lowest resonant mode, l_D is $\lambda/2$. Thus, λ_L is $2l_D$. The fractional bandwidth can be calculated through

$$BW = 2\frac{\lambda_L - \lambda_H}{\lambda_L + \lambda_H}, \tag{4}$$

where BW is the expanded bandwidth [7]. Bringing λ_L and λ_H into (4), the BW is calculated as 30%, where compared with the initial SWBA, the paralleling process will expand at least an extra 30% bandwidth toward the low frequency range of the band of interest. The actual obtained BW is larger than 30% because l_D is generally less than $\lambda/2$ when BD is working in the lowest resonant mode. The current distribution after applying the parallel connection of the SWBA and the X-shape BD is shown in Fig. 2(f), where region R is removed to reduce the gain degradation caused by the reversed currents toward the upper limit of the band of interest.

Basically, the broadside gain in the broadband (below 5 GHz) has been enhanced, and the impedance bandwidth has been extended to lower frequencies. However, the low value of the gain at high frequency (6 GHz) due to the LEW remains a limitation. This will be solved by the ORC, which not only suppresses the LEW but also increases the broadside gain.

III. CONFIGURATION AND OPERATING MECHANISM

A. ANTENNA CONFIGURATION

The configuration of the proposed antenna is illustrated in Fig. 3, where $L_1 = 24.6$ mm, $L_2 = 31.9$ mm, $W_1 = 26.7$ mm, and $W_2 = 26.6$ mm. The antenna consists of a F4B

($\varepsilon_r = 2.65$, $\delta = 0.001$) substrate layer (Sub2) and two FR4 ($\varepsilon_r = 4.4$, $\delta = 0.01$) substrate layers (Sub1 and Sub3) highlighted in Fig. 3(e). The excited element developed in Section II is etched on the upper side of Sub 2 (thickness of 2 mm). As shown in the figure, to form the ORC, the four patches (P_1, P_2, P_3 and, P_4) are etched on Sub1 and Sub3 (thicknesses of 1 mm), where P_1 and P_3 are right above P_2 and P_4. Considering both the impedance matching and the ORC performance, the distances between the patches and the excited element are set 9 mm, leading to the distances of Sub1-to-Sub2 and Sub2-to-Sub3 of 9 mm and 7 mm, respectively.

Shown in Fig. 3(a), N and N1 are two symmetric points on the metal edges along the taper slot, where the currents are denoted as J_1 and J_2. When the antenna is balanced fed, J_1 and J_2 are equal in amplitude and opposite in phase. J_1 and J_2 can be decomposed into J_{1c} and J_{1d}, and J_{2c} and J_{2d}, respectively. J_{1c} and J_{2c} are common mode (CM) currents contributing to the radiation, whereas J_{1d} and J_{2d} are differential mode (DM) currents driving the propagation of the TEM wave within the taper slot, which is the operating mechanism of the antenna in the high frequency leakage mode.

B. DESIGN AND WORKING MECHANISM OF ORC

The ORC that can simultaneously enhance the broadside gain and choke the end-fire travelling wave is introduced to solve the gain depression at 6 GHz due to the LEW. In the ORC, each patch, which simultaneously functions as a broadside radiator and an end-fire choke, can be divided into two areas, i.e., A_1 and B_1 for P_1 shown in Fig. 3(d). A_1 and A_2 are placed above and below the active element along the first portion of the taper slot. The same occurs for the symmetric patches P_3 and P_4. The area A acts as TM_{10} mode resonating patch antenna at 6 GHz enhancing the broadside (+/− z) radiation. The area B of the two patches P_1 and P_2 works as a choke for the LEW within the taper slot, thus suppressing the end-fire (+/− y) radiation. The function of ORC is realized through designing of the patches and the slot on the ground, where the ground is also the excited element.

1) RADIATING PART OF ORC

The patch area A has a relatively complete ground, where the width of the slot is shorter than the edge of the patch (L_1). The patch area A can be designed as a patch antenna with the slot acting as the source. Its TM_{10} operating mode improves the broadside radiation compared to higher order modes of the patch being characterized by strong sidelobes [19]–[21]. The resonant frequency of the area A working at the TM_{10} resonant mode can be easily expressed as

$$f = \frac{v_0}{2L\sqrt{\varepsilon_r}} \tag{5}$$

following the cavity analysis method of patch antennas [22], where v_0 is the speed of light and $\varepsilon_r = 1$ is the free space

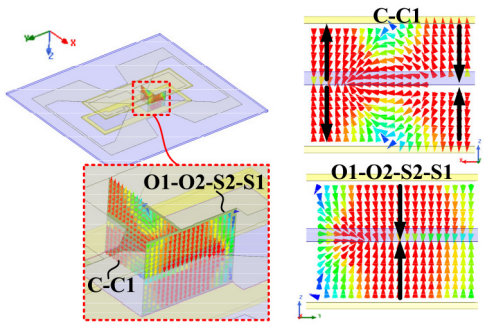

FIGURE 4. E-field distributions on C-C1 plane and O1-O2-S2-S1 plane at 6 GHz.

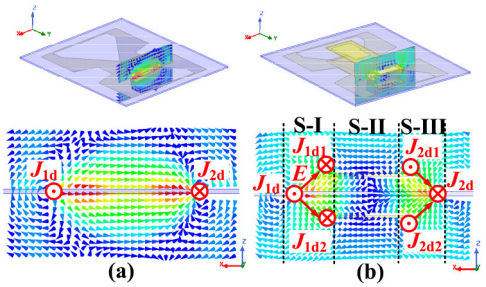

FIGURE 5. E-field distributions on D-D1 plane at 6 GHz. (a) Without patches. (b) With patches.

permittivity due to the air between the patches and the active element. Eq. (5) holds when the walls along the perimeter of the patch can be recognized as "magnetic wall" short-circuiting the TM wave, such as $H_x = 0$ in the O1-Q1-Q2-P2 plane in Fig. 3(c). By considering the polarization and the currents distribution of the excited element, the planes O1-Q1-Q2-P2, S1-R1-R2-S2, O3-Q3-Q4-P4, and S3-R3-R4-S4 satisfy the condition of the "magnetic wall". Thus, by applying (5) based on $f = 6$ GHz, the size of the patch area A is evaluated as $L_1 = 24.6$ mm according to Fig. 3(d). Fig. 4 shows the E-field distributions at 6 GHz on the C-C1 cut plane and on the O1-O2-S2-S1 plane defined in Fig. 3(a) and Fig. 3(c), respectively. From the figure it is evident that the patch is resonating following the E-field pattern of the TM_{10} resonant mode, as expected.

2) CHOKING PART OF ORC

The area B of the patch has no complete ground directly beneath, thus it cannot act as a resonant radiating structure. The patch works as a waveguide for the LEW together with the edges of the slot. Fig. 5 shows the E-field distributions on the D-D1 cut plane at 6 GHz in two cases, with and without the patches. As mentioned above, the propagation of the TEM wave is driven by the differential currents J_{1d} and J_{2d}, through which the currents J_{1d1}, J_{1d2}, J_{2d1}, and J_{2d2} are induced on the edges of the patches as shown in Fig. 5(b). In region S-I, J_{1d1} and J_{1d2} are currents flowing in opposite direction with respect to J_{1d}. A waveguide is formed by J_{1d}, J_{1d1}, and J_{1d2}. A similar current configuration occurs in region S-III, where a waveguide is formed by J_{1d}, J_{2d1}, and J_{2d2}. In region S-II, the E-field induced by J_{1d} and J_{2d}

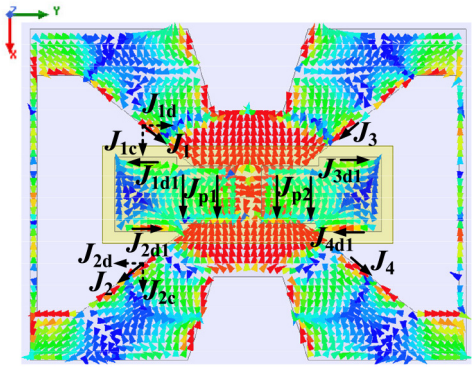

FIGURE 6. Simulated current distributions of the antenna at 6 GHz.

on the patches satisfy the condition in (6)

$$\hat{n} \times \vec{E} = 0, \tag{6}$$

where the tangential components of $E^{\rightarrow}$ are "shorted out". The normal components of $E^{\rightarrow}$ generated by J_{1d} and J_{2d} are out-of-phase leading to a E-field depression on the patches. In the vicinity of the patches of region S-II, the E-field generated by J_{1d} is cancelled by that generated by J_{1d1} and J_{1d2}, similarly to what happens for the case of J_{2d}, J_{2d1}, and J_{2d2} currents. Thus, the taper slot is turned from the initial TEM waveguide into the two waveguides in regions S-I and S-III. The waves propagate through the two waveguides up to the end of the patches, where the waveguides are open circuited. Therefore, the travelling wave in the taper slot are suppressed by the patches.

IV. SIMULATION DISCUSSIONS

Fig. 6 shows the simulated currents on the proposed antenna at 6 GHz. The currents J_{pn} ($n = 1, 2, 3, 4$) in region A comply with that of the microstrip patch acting as a TM_{10} mode resonator, which again proves the intended operating mode of the added patch A. The direction of the currents J_{ndm} ($n = 1, 2, 3, 4$; $m = 1, 2$) is the same as the corresponding currents J_{nd}, since they both flows along the y-axis, whereas J_{ndm} is opposite with respect to J_{nd}. The patch in region B_n contributes more to the wave guided in the $+/-$ y directions and less to the radiation along the $+/-$ z directions. The E-field distributions on the L-L1 cut-plane at 6 GHz with and without patches are shown in Fig. 7(a). From the figure, it is shown how the patches enhance the broadside radiation while decreasing the end-fire radiation. Fig. 7(b) shows the H-plane (L-L1 plane) patterns at 6 GHz in the cases without and with patches. The presence of the patches enhances the gain in the $+/-$ z directions by 13.1 dB, whereas the gain in $+/-$ y directions decreases by 4.5 dB. This validates the advantage of the ORC.

Fig. 8 shows the $|S_{11}|$ results of the proposed antenna, of the excited element, of the X-shape BD, and of the SWBA. From the figure, the half-wavelength resonance of

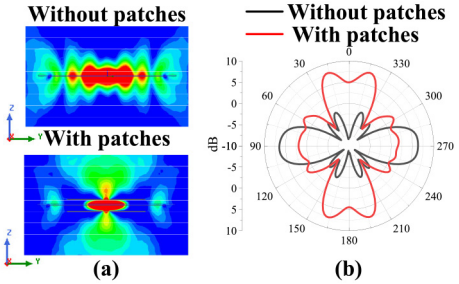

FIGURE 7. (a) E-field distributions on H-plane (L-L1 plane) at 6 GHz in cases of without with patches; (b) H-plane (L-L1 plane) patterns at 6 GHz in cases of without and with patches.

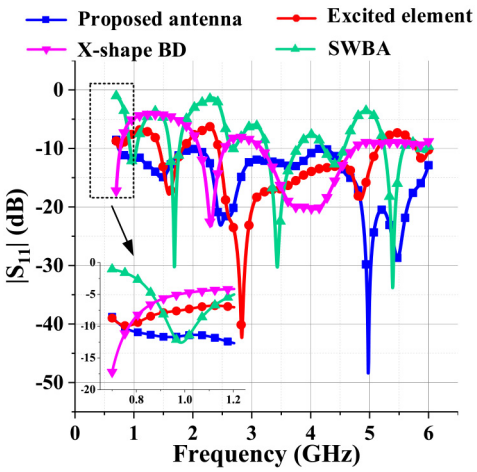

FIGURE 8. The simulated $|S_{11}|$ of the proposed antenna, the excited element, the X-shape BD, and the SWBA.

the X shape BD is about 700 MHz. The one wavelength SWBA operates at 0.98 GHz, below which frequency the SWBA is mismatched due to the low radiation resistance. Compared with the SWBA, the active element achieves a better impedance matching performance at 0.7 GHz due to the introduction of X-shape BD. The matching characteristic of the proposed antenna within the 0.7-0.98 GHz band is further improved by introducing the patches since they help decreasing the quality factor of the resonance. At high frequencies, the patches bring a capacitive load to the input impedance that improves the matching performance.

The broadside gain curves of the proposed antenna, of the excited element, of the X-shape BD, and of the SWBA are shown in Fig. 9. The X-shape BD is characterized by a gain notch occurring within 3-3.4 GHz due to the gain cancellation by the reverse currents. A good complementary property is shown in the broadband gains of the SWBA and the BD, as already analyzed in Section II. The excited element has a gain depression near 6 GHz. However, with the introduction of the patch, the gain is enhanced by the slot-fed patch. Finally, the proposed antenna obtains a gain of 3-8 dBi over the entire working band realizing a 158% effective bandwidth, calculated from 700 MHz to 6 GHz, in the broadside radiation direction.

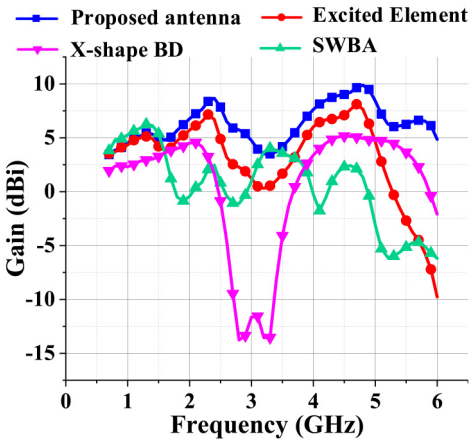

FIGURE 9. The simulated gains of the proposed antenna, the excited element, the X-shape BD, and the SWBA.

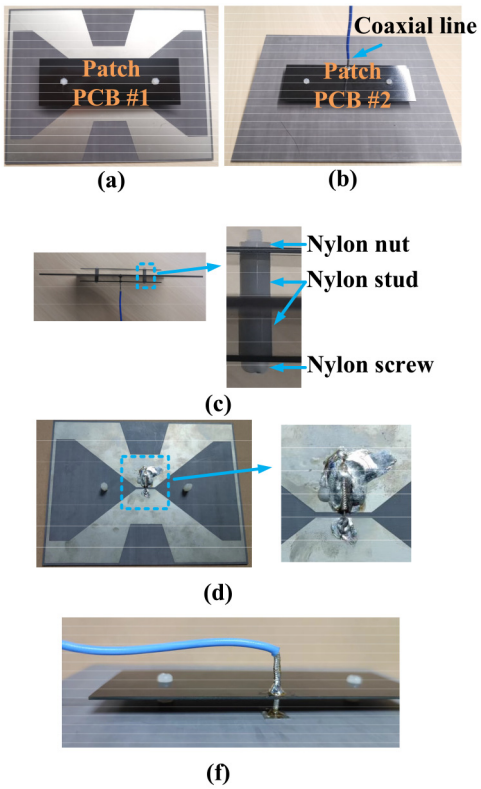

FIGURE 10. The photos of the prototype of the proposed antenna.

V. RESULTS AND DISCUSSION

Fig. 10 shows photographs of the prototype of the proposed antenna. The antenna mainly consists of three parts, the radiating element, the patch, and the input coaxial wire. The three parts are connected together by nylon screws, nylon studs and nylon nuts.

Fig. 11 shows the simulated and measured $|S_{11}|$ results. Within a band from 730 MHz to 6 GHz (156.6% fractional bandwidth), the simulated $|S_{11}|$ is less than -10 dB. The return loss is slightly worse from 700 MHz to 730 MHz where the simulated $|S_{11}|$ is lower than -8.9 dB. The trend of simulation curve is consistent with that of measured

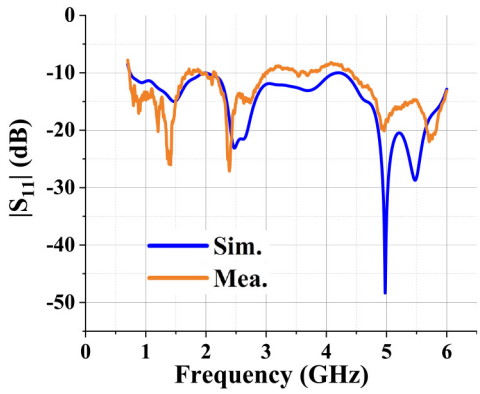

FIGURE 11. The measured and simulated results of $|S_{11}|$.

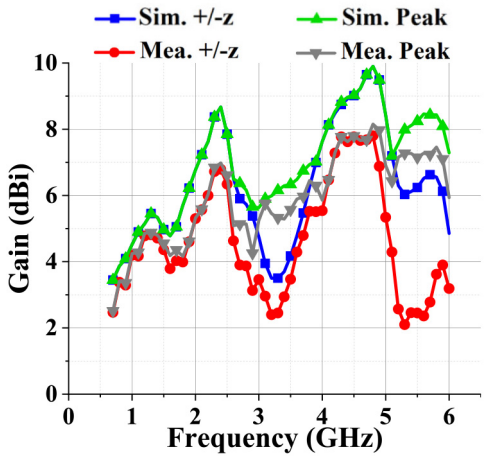

FIGURE 12. The measured and simulated peak gain and gain in the direction of $+/-z$.

curve. The measured results are higher than -10 dB in some frequencies. The worst measured $|S_{11}|$ is obtained at around 700 MHz where the $|S_{11}|$ reaches -7.8 dB.

The simulated and measured peak gain and gain in the $+/-$ z directions are shown in Fig. 12. The simulated and measured gains are 3.4-9.9 dBi and 2.1-7.8 dBi, respectively, whereas the simulated and measured peak gains are 3.4-9.9 dBi and 2.5-8.2 dBi, respectively in the whole band. Fig. 13 show the simulated and measured radiating efficiency. The simulated efficiency does not include return loss of the antenna and the contribution of the common mode current. The measured efficiency is 62%-100%. The discrepancies between the simulated and measured results are caused by the return loss, the errors in fabrications, common mode current contributions, and the uncertainties in measurements.

Fig. 14 shows the simulated and measured radiation pattern results on the E-plane and H-plane at 700 MHz, 2 GHz, and 6 GHz. Although good agreement is obtained, there are some differences. The discrepancies between the simulated and the measured results come from the manufacturing and assembly processes, and from the effect of common mode currents on flowing the outer shield of the coaxial line. As is seen in the Figure, the patterns are not in a stable shape

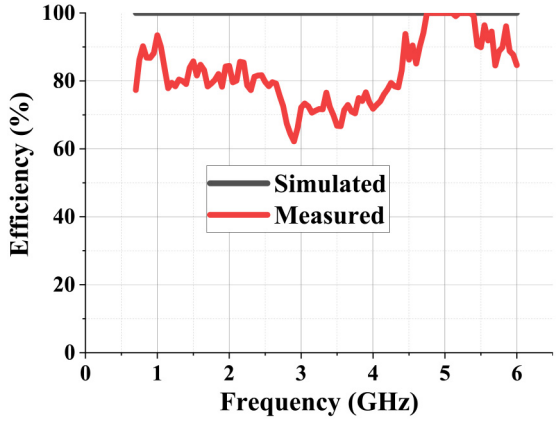

FIGURE 13. The measured and simulated radiating efficiency.

TABLE 1. Units for magnetic properties.

Ref.	BW	Dimension (λ_L^3)	Peak gain (dBi)	+/- z gain (dBi)
[2]	96%	0.397*0.096*0.015	1.8~3.7	1.8-3.7
[3]	110%	0.935*0.935*0.008	1.9~5.1	1.9-5.1
[9]	103%	0.348*0.273*0.006	4.0~5.3	4.0-5.3
[10]	58%	0.339*0.254*0.001	2.3~6.3	2.3-6.3
[11]	118%	0.374*0.168*0.07	0.5~6.2	-2.2-4.9
[14]	129%	0.298*0.293*0.009	-2.0~-6.0	NA
[15]	131%	1.110*0.389*0.006	2.1~7.3	2.1~7.3
proposed	158%	0.435*0.329*0.044	2.5~8.2	2.1-7.8

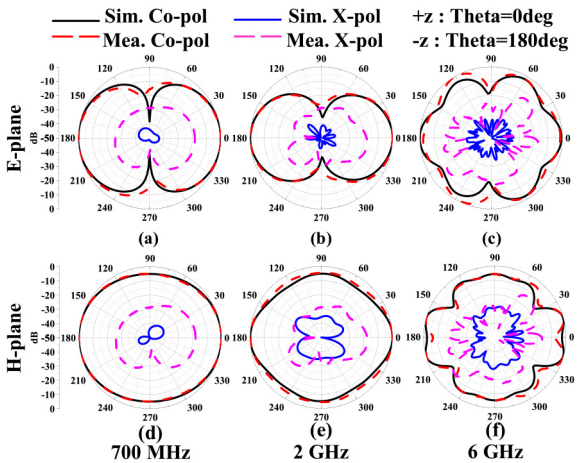

FIGURE 14. The simulated and measured pattern results of E-plane and H-plane at 700 MHz, 2 GHz, and 6 GHz.

over the operating bandwidth. This is due to the current distributions vary greatly in such a wide band. The problem deserves further research.

Table 1 shows the comparison of the proposed antenna with other antennas designed for similar applications and based on similar requirements. The proposed antenna shows an advantage in terms of bandwidth of the effective gain in the broadside +/− z directions over the others.

VI. CONCLUSION

A compact broadband antenna is proposed in this paper, which is able to achieve a larger than 2 dBi broadside gain in the +/− z directions over a 158% fractional bandwidth from 700 MHz to 6 GHz. The performances are obtained through solving the gain degradations caused by the CRC and the LEW. To deal with the CRC, a concept of complementary gains is proposed and implemented through accurately analyzing the resonant modes of the two paralleling antennas of the SWBA and the X-shape BD, where a design equation is given determining the relationship between the slot size and the dimension of the metal outline. The ORC is presented to solve the gain depression due to the LEW through simultaneously enhancing the broadside gain and choking the end-fire travelling wave. In the ORC, each one patch acts as both the TM_{10} mode microstrip antenna in the broadside and the choke of the end-fire travelling wave. With the help of the ORC, the gain in +/− z directions is enhanced by 13.1 dB at 6 GHz compared to that without the ORC, thus further increasing the operating band at high frequencies. Finally, a measured peak gain of 2.5-8.2 dBi and a measured gain of 2.1-7.8 dBi in +/− z directions are achieved in the bandwidth of 700 MHz – 6 GHz (158%). Both the concepts of the complementary gains and the ORC and the insight of the problems, which are the CRC and the LEW, in realizing an effective wideband broadside radiating performance may be enlightened for the future designs of broadside antennas to realize wider bandwidth. The proposed antenna is believed a potential solution for various wideband broadside radiating applications.

REFERENCES

[1] J. Sun and K.-M. Luk, "A fully transparent wideband water patch antenna with L-shaped feed," *IEEE Open J. Antennas Propag.*, vol. 2, pp. 968–975, 2021.

[2] F. Gao, F. Zhang, L. Lu, T. Ni, and Y. Jiao, "Low-profile dipole antenna with enhanced impedance and gain performance for wideband wireless applications," *IEEE Antennas Wireless Propag. Lett.*, vol. 12, pp. 372–375, 2013.

[3] Chair, Kishk, and Lee, "Ultrawide-band coplanar waveguide-fed rectangular slot antenna," *IEEE Antennas Wireless Propag. Lett.*, vol. 3, pp. 227–229, 2004.

[4] L. Wan, Z. Guo, and X. Chen, "Enabling efficient 5G NR and 4G LTE coexistence," *IEEE Wireless Commun.*, vol. 26, no. 1, pp. 6–8, Feb. 2019.

[5] A. M. Yacoub, M. O. Khalifa, and D. N. Aloi, "Wide band raised printed monopole for automotive 5G wireless communications," *IEEE Open J. Antennas Propag.*, vol. 3, pp. 502–510, 2022.

[6] Z. Wang, Y. Ning, and Y. Dong, "Compact shared aperture Quasi-Yagi antenna with pattern diversity for 5G-NR applications," *IEEE Trans. Antennas Propag.*, vol. 69, no. 7, pp. 4178–4183, Jul. 2021.

[7] J. D. Kraus and R. J. Marhefka, *Antennas for All Applications*. New York, NY, USA: McGraw-Hill, 2003.

[8] G. H. Brown, "Directional antennas," *Proc. IRE*, vol. 25, no. 1, pp. 78–145, Jan. 1937.

[9] G. Pan, Y. Li, Z. Zhang, and Z. Feng, "A compact wideband slot-loop hybrid antenna with a monopole feed," *IEEE Trans. Antennas Propag.*, vol. 62, no. 7, pp. 3864–3868, Jul. 2014.

[10] M. O. Sallam, S. M. Kandil, V. Volski, G. A. E. Vandenbosch, and E. A. Soliman, "Wideband CPW-fed flexible bow-tie slot antenna for WLAN/WiMax systems," *IEEE Trans. Antennas Propag.*, vol. 65, no. 8, pp. 4274–4277, Aug. 2017.

[11] X. N. Low, Z. N. Chen, and T. S. P. See, "A UWB dipole antenna with enhanced impedance and gain performance," *IEEE Trans. Antennas Propag.*, vol. 57, no. 10, pp. 2959–2966, Oct. 2009.
[12] Y.-C. Lin and K.-J. Hung, "Compact ultrawideband rectangular aperture antenna and band-notched designs," *IEEE Trans. Antennas Propag.*, vol. 54, no. 11, pp. 3075–3081, Nov. 2006.
[13] M. R. Nikkhah, A. A. Kishk, and J. Rashed-Mohassel, "Wideband DRA array placed on array of slot windows," *IEEE Trans. Antennas Propag.*, vol. 63, no. 12, pp. 5382–5390, Dec. 2015.
[14] W.-J. Lu, W.-H. Zhang, K. F. Tong, and H.-B. Zhu, "Planar wideband loop-dipole composite antenna," *IEEE Trans. Antennas Propag.*, vol. 62, no. 4, pp. 2275–2279, Apr. 2014.
[15] M. Li, Y. Zhang, and M.-C. Tang, "Design of a compact, wideband, bidirectional antenna using index-gradient patches," *IEEE Antennas Wireless Propag. Lett.*, vol. 17, pp. 1218–1222, 2018.
[16] L. Chi *et al.*, "Rugged linear array for IoT applications," *IEEE Internet Things J.*, vol. 7, no. 6, pp. 5078–5087, Jun. 2020.
[17] S. A. Schelkunoff, "Theory of antennas of arbitrary size and shape," *Proc. IRE*, vol. 29, no. 9, pp. 493–521, Sep. 1941.
[18] W. Song, Z. Weng, Y.-C. Jiao, L. Wang, and H.-W. Yu, "Omnidirectional WLAN antenna with common-mode current suppression," *IEEE Trans. Antennas Propag.*, vol. 69, no. 9, pp. 5980–5985, Sep. 2021.
[19] T. H. Jang, H. Y. Kim, I. S. Song, C. J. Lee, J. H. Lee, and C. S. Park, "A wideband aperture efficient 60-GHz series-fed E-shaped patch antenna array with copolarized parasitic patches," *IEEE Trans. Antennas Propag.*, vol. 64, no. 12, pp. 5518–5521, Dec. 2016.
[20] D.-F. Guan, Y.-S. Zhang, Z.-P. Qian, Y. Li, W. Cao, and F. Yuan, "Compact microstrip patch array antenna with parasitically coupled feed," *IEEE Trans. Antennas Propag.*, vol. 64, no. 6, pp. 2531–2534, Jun. 2016.
[21] K.-Z. Hu, M.-C. Tang, D. Li, Y. Wang, and M. Li, "Design of compact, single-layered substrate integrated waveguide filtenna with parasitic patch," *IEEE Trans. Antennas Propag.*, vol. 68, no. 2, pp. 1134–1139, Feb. 2020.
[22] C. A. Balanis, *Antenna Theory: Analysis and Design*. Chichester, U.K.: Wiley, 2015.

LIDONG CHI (Graduate Student Member, IEEE) received the B.S. and M.S. degrees in electronic information and technology from Hunan University, Changsha, China, in 2014 and 2017, respectively, where he is currently pursuing the Ph.D. degree in electronics. His research interests include end-fire directional antennas, millimeter-wave antennas, antenna arrays, and antenna-in-package.

YIHONG QI (Senior Member, IEEE) received the Ph.D. degree in electronics from Xidian University, Xi'an, China.

He was an Associate Professor with Southeast University, Nanjing, China. From 1995 to 2010, he was with Research in Motion (Blackberry), Waterloo, ON, Canada, where he was the Director of Advanced Electromagnetic Research. He is currently the President of Link-E, Zhuhai, China; the President and the Chief Scientist with General Test Systems, Inc., Shenzhen, China. He is also an Adjunct Professor with the EMC Laboratory, Missouri University of Science and Technology, Rolla, MO, USA, an Adjunct Professor with Western University, London, Canada, and an Adjunct Professor with Hunan University, Changsha, China. He is an Honorary Professor with Southwest Jiaotong University and Xidian, China. He is an inventor of more than 500 published and pending patents. He has received an IEEE EMC Society Technical Achievement Award in August 2017. He was a Distinguished Lecturer of IEEE EMC Society and the founding Chairman of the IEEE EMC TC-12. He is a Fellow of Canadian Academy of Engineering and Fellow of National Academy of Inventors.

FRANCESCO DE PAULIS (Senior Member, IEEE) was born in L'Aquila, Italy, in 1981. He received the specialist degree *(summa cum laude)* in electronic engineering from the University of L'Aquila, L'Aquila, in 2006, the M.S. degree in electrical engineering from the EMC Laboratory, Missouri University of Science and Technology (formerly, University of Missouri–Rolla), Rolla, MO, USA, in May 2008, and the Ph.D. degree in electrical and information engineering from the University of L'Aquila in 2012.

In August 2006, he joined EMC Laboratory, Missouri University of Science and Technology (formerly, University of Missouri–Rolla). From August 2004 to August 2006, he was involved in research activities with the UAq EMC Laboratory, L'Aquila, and from August 2006 to May 2008, the MST EMC Laboratory. From June 2004 to June 2005, he interned with Selex Communications, L'Aquila (currently, Leonardo s.p.a.), within the layout/SI/PI design group. He is currently a Researcher with the UAq EMC Laboratory. His current research interests include SI/PI design on PCB, packages interposers and chips, analysis and characterization of composite materials for shielding and absorption, RF interference in mixed-signal system, TSVs in silicon chips and interposers, EMI problem investigation, EMC measurements based on NF-FF transformation techniques, remote fault detection in transmission lines, and design of T/R modules and electronic systems for space applications. He was the recipient of the Past President's Memorial Award from the IEEE EMC Society in 2010, the Best Paper Award in 2010, 2013, and 2016, the Best Student Paper Award in 2009 and 2011 at the IEEE International Symposium on EMC, and the Paper Award in the power and RF design category in 2010, 2011, and 2012 at the IEC DesignCon. He received the Honorable Mention for the Best Paper Award of the Transaction on EMC in 2014. He was selected as a Distinguished Reviewer of the IEEE TRANSACTIONS ON ELECTROMAGNETIC COMPATIBILITY for the years 2014 and 2016. He was an Associate Editor for the IEEE TRANSACTIONS ON ELECTROMAGNETIC COMPATIBILITY for a 2-year term from January 2017 to March 2019.

YUEPING ZHANG (Fellow, IEEE) is a Full Professor with the School of Electrical and Electronic Engineering, Nanyang Technological University, Singapore. He holds seven U.S. patents. He has made pioneering and significant contributions to the development of AiP technology. He was conferred the Distinguished Scholar affiliated to Shanghai Jiao Tong University, China, in 2012. He was awarded a William Mong Visiting Fellowship in 2005 and appointed as a Visiting Professor by the University of Hong Kong, China, in 2014. He has published numerous papers, including two invited and one regular papers in the Proceedings of the IEEE and one invited paper in the IEEE TRANSACTIONS ON ANTENNAS AND PROPAGATION. He is the only Chinese radio scientist who has managed to publish a historical article in an English learned journal such as the *IEEE Antennas and Propagation Magazine*. His current research interests include the development of antennaon-chip technology for very large-scale antenna integration and characterization of chip-scale propagation channels at terahertz for wireless chip area network.

Prof. Zhang received the Best Paper Award from the 2nd IEEE/IET International Symposium on Communication Systems, Networks and Digital Signal Processing, July 18–20, 2000, Bournemouth, U.K., the Best Paper Prize from the 3rd IEEE International Workshop on Antenna Technology, March 21–23, 2007, Cambridge, U.K., and the Best Paper Award from the 10th IEEE Global Symposium on Millimetre-Waves, May 24–26, 2017, Hong Kong, China. He received the Sergei A. Schelkunoff Prize Paper Award from the IEEE AP-S in 2012. He received the John Kraus Antenna Award from the IEEE AP-S in 2020. He is a Distinguished Lecturer of the IEEE Antennas and Propagation Society (IEEE AP-S) and a member of the IEEE AP-S Paper Award Committee. He was a Member of the IEEE AP-S Field Award Committee from 2015 to 2017, an Associate Editor of the IEEE TRANSACTIONS ON ANTENNAS AND PROPAGATION from 2010 to 2016, and the Chair of the IEEE Singapore MTT/AP joint Chapter in 2012.